



ORIGINAL ARTICLE

Particle atomic layer deposition of alumina for sintering yttria-stabilized cubic zirconia

Rebecca J. O'Toole¹ | Christopher J. Bartel¹ | Maila U. Kodas¹ | Alexa J. Horrell¹ | Sandrine Ricote² | Neal P. Sullivan² | Christopher J. Gump³ | Charles B. Musgrave^{1,4,5,6} | Alan W. Weimer¹

¹Department of Chemical and Biological Engineering, University of Colorado Boulder, Boulder, Colorado

²Department of Mechanical Engineering, Colorado Fuel Cell Center, Colorado School of Mines, Golden, Colorado

³ALD NanoSolutions, Inc., Broomfield, Colorado

⁴Department of Chemistry and Biochemistry, University of Colorado Boulder, Boulder, Colorado

⁵Materials Science and Engineering Program, University of Colorado Boulder, Boulder, Colorado

⁶Materials and Chemical Science and Technology, National Renewable Energy Laboratory, Golden, Colorado

Correspondence

Alan W. Weimer, Department of Chemical and Biological Engineering, University of Colorado Boulder, Boulder, Colorado.
Email: alan.weimer@colorado.edu

Funding information

National Science Foundation, Grant/Award Number: 1563537

Abstract

The addition of aluminum oxide (Al_2O_3) as a sintering aid to yttria-stabilized zirconia (YSZ) reduces the required densification temperature. Sintering aids are incorporated using a number of processes which can lead to ambiguity when determining the effect of the sintering aid on the densification mechanism. In this study, a novel method for sintering aid addition, Particle Atomic Layer Deposition (ALD), was used to deposit an amorphous Al_2O_3 thin film on YSZ particles. Transmission electron microscopy confirmed the deposition of conformal Al_2O_3 thin films on the surface of the YSZ particles. The addition of Al_2O_3 to YSZ reduced the temperature at which densification began by $\sim 75^\circ\text{C}$, and 2.2 wt% Al_2O_3 addition resulted in a minimum activation energy for the intermediate stage of densification. This concentration is well in excess of the solubility limit of Al_2O_3 in YSZ, showing that Al_2O_3 does not enhance the densification of YSZ solely by dissolving into the YSZ lattice and activating volume diffusion. The addition of 0.7 wt% Al_2O_3 with one Particle ALD cycle enhanced the ionic conductivity of YSZ by 23% after sintering at 1350°C for 2 hours, demonstrating that dense parts with high oxygen ion conductivities can be produced after sintering at reduced temperatures. One Particle ALD cycle is a fast, easily scaled-up process that eliminates the use of solvents and has substantial cost/performance advantages over conventional processing.

1 | INTRODUCTION

The incorporation of 8 mol% yttrium oxide (Y_2O_3) into zirconium oxide (ZrO_2) optimally stabilizes the ionically conductive cubic phase of ZrO_2 (yttria-stabilized cubic zirconia, YSZ), which is studied extensively for applications as an electrolyte in solid oxide fuel cells (SOFC) and other electrochemical devices.^{1–5} While YSZ is an attractive oxygen ion conductor for these applications, commercialization is

hindered in part by the high sintering temperature ($\sim 1450^\circ\text{C}$) required to facilitate diffusion of slow Zr^{4+} cations and reach near theoretical density.⁶ The incorporation of small amounts of aluminum oxide (Al_2O_3) as a sintering aid decreases the sintering temperature required to reach near-theoretical density without deleteriously affecting the key dense part properties such as ionic conductivity^{7–11} and mechanical strength.^{12,13} The role of Al_2O_3 in decreasing the required sintering temperature is typically attributed to the dissolution of Al_2O_3 into YSZ grains, resulting in a change in the Zr^{4+} cation diffusion mechanism from grain-boundary diffusion

O'Toole and Bartel contributed equally.

(GBD) to volume diffusion (VD).^{14,15} However, Suárez and Sakka¹⁵ showed that the beneficial effects of Al₂O₃ continue at concentrations at least as high as 2.16 wt% Al₂O₃, significantly above the reported solubility of <0.3 to 1 wt% Al₂O₃ in ZrO₂ or YSZ,^{9,16–18} suggesting that the dissolution of Al₂O₃ into the YSZ lattice is not the only cause of enhanced YSZ densification.

Sintering aids are incorporated to promote densification at reduced temperatures by changing the mechanism of sintering (eg, solid-state to liquid phase) and/or increasing the diffusion coefficient of migrating ions.^{19,20} The dispersion of sintering aid within the primary ceramic is critical to the performance of the additive and is typically achieved using milling,^{10,21} spray drying, and/or colloidal processing.^{11,22–24} However, these methods can result in localized regions of excess or deficient sintering aid which can reduce the homogeneity of the final microstructure and adversely affect material properties.^{25,26} In this work, we use a novel process for sintering aid addition, atomic layer deposition (ALD),²⁷ to precisely coat individual YSZ particles with a desired thickness of amorphous Al₂O₃. ALD enables the deposition of uniform ceramic (or hybrid organic/inorganic) thin films on either flat or particle substrates and has applications in many fields including semiconductor manufacturing,²⁸ catalysis,²⁹ and batteries.³⁰ Particle ALD (ie, ALD on a particle substrate) for sintering aid incorporation homogeneously deposits the desired amount of sintering aid, reducing the variability associated with conventional sintering aid incorporation techniques which clarifies the effect of sintering aid location, phase, and quantity on densification phenomena. This is the first work to investigate Particle ALD as a route to enhance ceramic sintering and microstructural homogeneity.

2 | EXPERIMENTAL

2.1 | Powder sample preparation

Commercial YSZ prepared by the hydrolysis method with 13.30 wt% Y₂O₃ and ≤0.10 wt % Al₂O₃ (>99.7 wt% ZrO₂ + HfO₂ + Y₂O₃, 12.69 m²/g specific surface area) was purchased from Tosoh (TZ-8Y). This sample (0ALD, where 0 refers to the number of ALD cycles) was used as the ALD substrate and also for comparison to all samples with Al₂O₃. A quantity of 500 g of substrate (0ALD) were loaded into a 500 mL fluidized bed ALD reactor and dried at 180°C and ~10 torr of nitrogen for 4 hours. Subsequently, the substrate powder bed was coated with Al₂O₃ by ALD at varying thicknesses, controlled by the number of ALD cycles.³¹ The sequential exposure of the substrate to trimethyl aluminum (TMA, Al(CH₃)₃) and water (with inert nitrogen purge between) constitutes a single ALD cycle.³² The substrate was coated by an amorphous Al₂O₃ film of varying thicknesses by varying the number of

cycles from 1 to 9 (1ALD, 3ALD, 5ALD, 7ALD, and 9ALD). To determine the effect of the Al₂O₃ structure (crystalline or amorphous) on densification, 40 g of 5ALD powder were calcined for 2 hours at 750°C to crystallize the Al₂O₃ film (CR).³³ For comparison of sintering aid incorporation by conventional mechanical mixing to incorporation by Particle ALD, 0ALD was also mixed with 2.2 wt% Al₂O₃ nanopowder (13 nm, 99.8% trace metal basis, Sigma-Aldrich) in a planetary mixer (Thinky Corp. AV-50LED) for 50 minutes at 400 rpm with ethanol and yttria-tetragonal zirconia polycrystal (Y-TZP, 3 mol% Y₂O₃-doped ZrO₂) milling media (Tosoh 5 mm YTZ Grinding Media) in an 11:2 media to powder ratio (this sample referred to as BM). The concentration of Al₂O₃ for all ALD-coated samples was measured using inductively coupled plasma optical emission spectroscopy (ICP-OES).

2.2 | Sintering experiments

Powder was mixed with a polymeric binder (Acros Organics, polyvinyl alcohol, 98%–98.8% hydrolyzed, ~31 000–50 000 g/mol) then uniaxially pressed for 90 seconds at 1 metric ton using a hydraulic press to form 6 mm diameter powder compacts. An average green density was determined for each sample type by geometric measurement, yielding average green densities ranging from 45% to 48% theoretical density. The green compacts were then used for constant rate of heating (CRH) dilatometer experiments in air. For each experiment, the temperature was increased from room temperature to 600°C at 1°C/min for the removal of binder, then from 600 to 1550°C at each of four heating rates—5, 10, 15, and 20°C/min. A horizontal push-rod dilatometer (Netzsch, DIL 402C) was used to precisely measure axial shrinkage over the duration of the CRH experiment. Isotropic shrinkage was assumed, and relative density was calculated as a function of temperature using Equation 1:

$$\rho(T) = \frac{\rho_0}{\rho_{th} \left(1 + \frac{\Delta L(T)}{L_0}\right)^3} \quad (1)$$

where $\rho(T)$ is the instantaneous relative density, ρ_0 is the green density of the sample, ρ_{th} is the theoretical density (6.10 g/cm³ for YSZ and 3.95 g/cm³ for Al₂O₃), $\Delta L(T)$ is the instantaneous length change, and L_0 is the initial length of the sample. The measured shrinkage was adjusted to account for the thermal expansion of the specimen by calculating the coefficient of thermal expansion from the slope of the cooling portion of the densification curve.³⁴

2.3 | Microstructural analysis

To characterize the as-deposited Al₂O₃ films, samples were ion milled (FEI Dual Beam FIB/SEM) and imaged using

high-resolution transmission electron microscopy (HRTEM; FEI Tecnai TF-20 FEG/TEM) and energy dispersive spectroscopy (EDS; Oxford INCA, Bruker Quantax) by EAG Laboratories. Scanning electron microscopy (SEM; Hitachi SU3500) was used to characterize the microstructure of samples at various relative densities. Prior to imaging, powder was mixed with a polymeric binder (Acros Organics, polyvinyl alcohol, 98%-98.8% hydrolyzed, ~31 000-50 000 g/mol) then uniaxially pressed for 90 seconds at 1 metric ton to form 13 mm diameter powder compacts. Samples were then sintered at 1150-1450°C for 0-2 hours and polished using diamond paste. Samples with a relative density >75% were thermally etched in air for 30 minutes at 50°C below the isothermal sintering temperature. The grain size of high-density (>90% relative density) and low-density (<75% relative density) samples was determined by direct measurement of the grain diameter. The grain size of medium density samples (between 75% and 90% relative density) was determined by the linear intercept method.³⁵

2.4 | Ionic conductivity analysis

Powder was mixed with a polymeric binder (3 wt% polyvinyl alcohol (Alfa Aesar, 87%-89% hydrolyzed, high molecular weight) in water) then uniaxially pressed for 10 seconds at 1.1 metric tons. Samples were then sintered at 1350°C for 2 hours and the final densities were measured geometrically. Next, samples were painted with Pt electrodes and annealed at 1000°C for 1 hour. Ionic conductivity measurements were performed in air for relevant SOFC operating temperatures (800-850°C) using AC impedance spectroscopy (Hewlett Packard 4284A Precision LCR Meter, 20 to 10⁶ Hz, 100 mV amplitude). Triplicate experiments were conducted for all sample types.

3 | RESULTS AND DISCUSSION

3.1 | Powder characterization

The concentration of Al₂O₃ as a function of the number of ALD cycles was determined by ICP-OES (Figure 1A) and used to calculate the approximate film thickness and growth rate from particle surface area, particle size, particle density, and film density. The growth rate of the Al₂O₃ film was estimated to be ~1 Å/cycle, similar to what others have observed for the Particle ALD of Al₂O₃,^{36,37} and found to be approximately linear with the cycle number. HRTEM and EDS revealed the presence of conformal, amorphous Al₂O₃ films that are approximately 1 nm in thickness for the 9ALD sample (Figure 1B-C). For lower cycle numbers, a monolayer or sub-monolayer, which cannot be resolved by HRTEM, is expected. The Brunauer-Emmett-Teller specific surface areas of 0-9ALD did not

differ significantly, supporting the assumption that chemical sintering of the YSZ particles did not occur during the ALD process (Table S1).

The addition of sintering aid via Particle ALD ensures a homogenous distribution of the additive with respect to the primary ceramic body (at least at the onset of densification). This homogeneous distribution controls for factors such as additive particle size, mixing, agglomeration, etc. and allows for a better understanding of the effects of the additive during densification. Because the Al₂O₃ film is deposited uniformly at the surface of each YSZ crystallite, the sintering aid is positioned to maximize the fraction of Al₂O₃ in contact with the YSZ surface, providing the shortest possible diffusion path into the YSZ grain interior and grain boundaries to enhance densification.

3.2 | Densification

Constant rate of heating experiments were conducted for all sample types at four heating rates (5, 10, 15, and 20°C/min) resulting in densification curves such as those shown in Figure 2A-B for the 10°C/min CRH experiments. Densification curves for all sample types and CRH experiments are plotted in Figure S1 of the Supporting Information. The

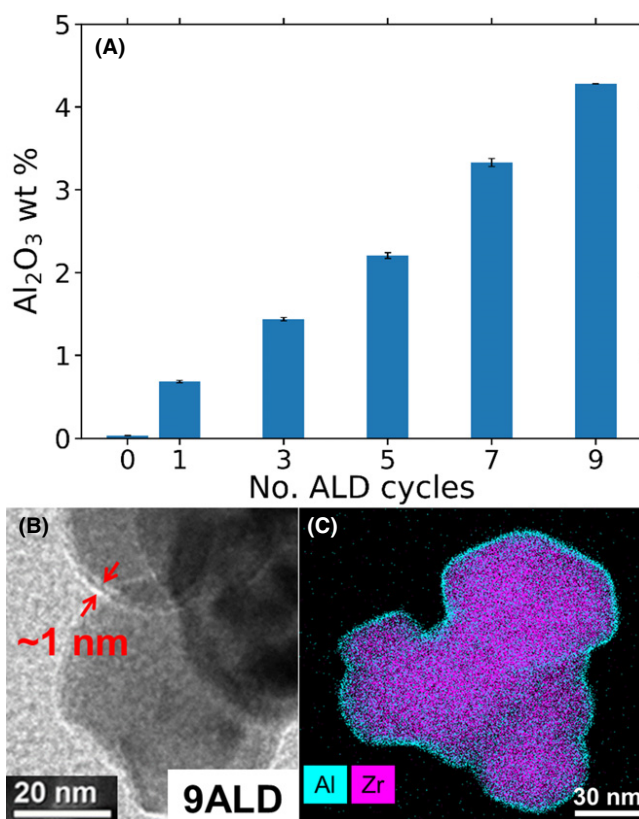


FIGURE 1 (A) Al₂O₃ concentration for all ALD samples measured using ICP-OES. (b) HRTEM of 9ALD and (C) EDS of 9ALD [Color figure can be viewed at wileyonlinelibrary.com]

densification curves show that the presence of Al_2O_3 (at all concentrations evaluated) decreases the temperature at which densification begins (ie where the densification rate exceeds 0.05 K^{-1}) by $\sim 75^\circ\text{C}$ compared with the control sample (0ALD). Densification rate vs temperature curves are shown in Figure 2C-D. Again, the presence of Al_2O_3 decreases the temperature at which the peak densification rate occurs by $\sim 100^\circ\text{C}$ compared with the control sample.

The initial stage of densification ($<60\%$ relative density) is dependent on particle-particle contact due to neck formation between adjacent YSZ particles. Based on Figure 2C, the presence of a pinhole-free Al_2O_3 film appears to impede this initial neck formation as the initial densification rate is lower for thicker films. Because the Al_2O_3 film blocks YSZ/YSZ contact, Al^{3+} cations in the Al_2O_3 film must diffuse away from between the YSZ particles to allow for neck formation to occur. 7ALD and 9ALD exhibit a reduction in initial densification rate relative to samples with a sub-monolayer Al_2O_3 film (1ALD, 3ALD) (Figure 2C, $<1200^\circ\text{C}$), which is commensurate with these samples possessing the thickest films evaluated (Al_2O_3 thickness $\sim 1 \text{ nm}$). Crystallization of the amorphous film prior to densification (CR) caused significant differences in the densification behavior relative to samples with an amorphous film (5ALD), so the Al_2O_3 films do not have sufficient time to crystallize before the onset of densification during dilatometer experiments. Crystallization of the amorphous Al_2O_3 film (CR) increases the structural order of the film, further hindering transport of Al^{3+} cations out of the Al_2O_3 film. This effect impedes neck formation during the initial stage of densification for the crystallized film

compared with the amorphous (as-deposited) film at the same concentration (Figure 2D, $<1100^\circ\text{C}$).

During the final stage of densification, grain growth and the consumption of isolated porosity are the dominant processes. If grain growth occurs too quickly, pores can break away from grain boundaries and become isolated within grains, and this intragranular porosity is resistant to densification and reduces the final density of the material.^{18,38,39} For samples with 2.2 wt% Al_2O_3 addition, the average grain size for BM and CR was greater than that of 5ALD (sintered at 1450°C for 2 hours; Figure 3B), while the final relative density of 5ALD was greater than that of BM and CR (sintered at 1550°C ; Figure 2B). This supports that enhanced grain growth in BM and CR caused pores to break away from grain boundaries, thereby reducing the final density of BM and CR relative to 5ALD. To confirm the phenomena observed for the BM sample, all CRH studies were replicated for the BM sample and found to be in good agreement with the results shown in Figure 2B (Figure S2, Table S2).

3.3 | Microstructure

The average grain size as a function of relative density for 0ALD, 3ALD, 5ALD, 7ALD, BM, and CR is shown in Figure 3A. During the initial and intermediate stages of densification ($<80\%$ relative density), average grain size for all samples remained approximately constant ($\sim 0.175 \mu\text{m}$). This was followed by significant grain growth during the final stage of densification ($>80\%$ relative density) and an increase in the average grain size to $>2 \mu\text{m}$. The addition of secondary phase particles can

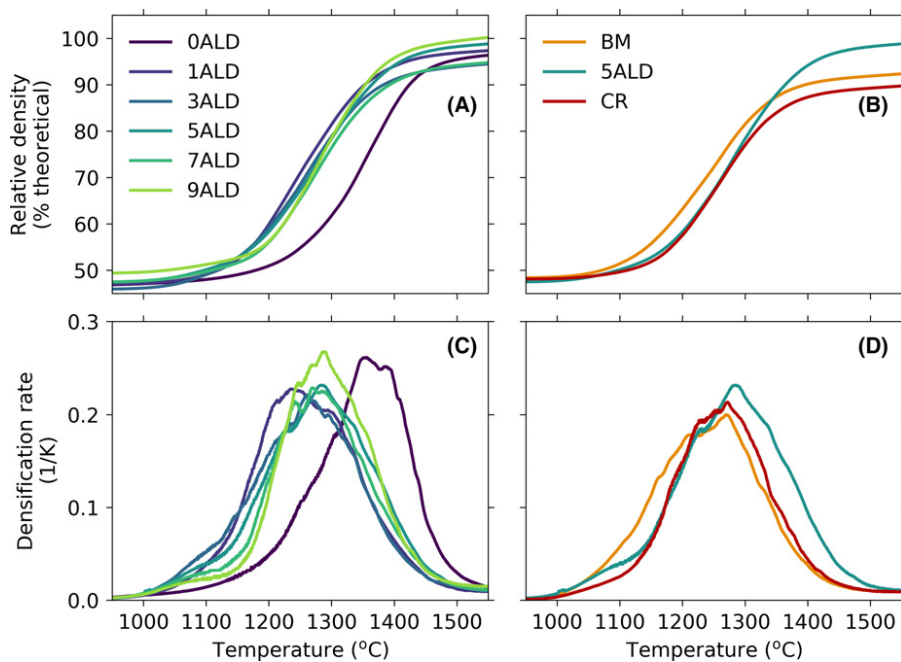
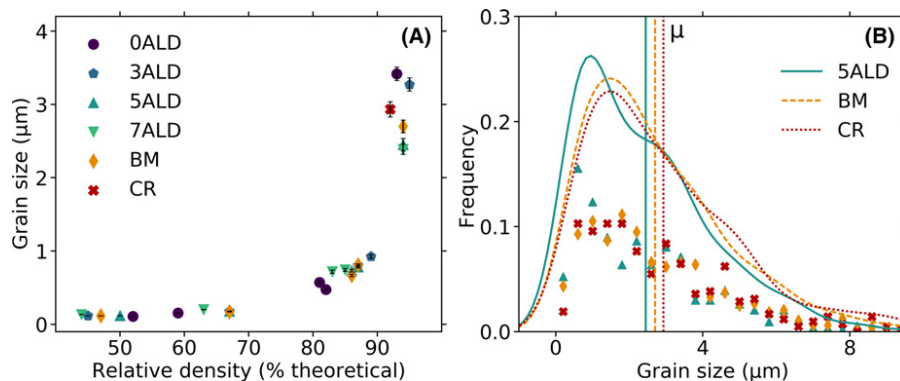


FIGURE 2 Relative density vs temperature for (A) 0-9ALD and (B) 5ALD (amorphous Al_2O_3 film), BM (ball milled), and CR (crystalline Al_2O_3 film) for the $10^\circ\text{C}/\text{min}$ CRH experiment and densification rate vs temperature for (C) 0-9ALD and (D) 5ALD, BM, and CR for the $10^\circ\text{C}/\text{min}$ CRH experiment [Color figure can be viewed at wileyonlinelibrary.com]

FIGURE 3 (A) The average grain size at various relative densities for 0ALD, 3ALD, 5ALD, 7ALD, BM, and CR. (B) The grain size distributions and kernel density estimations for 5ALD, BM, and CR, where μ indicates the mean grain size [Color figure can be viewed at wileyonlinelibrary.com]



reduce grain growth during the final stage of densification as a result of grain-boundary pinning.^{10,18,38,40} This effect is also observed for the ALD coated samples, where the final grain size decreases with increasing Al_2O_3 content. For 5ALD, BM, and CR (2.2 wt% Al_2O_3) at >92% relative density, the grain size distributions and average grain sizes were determined by direct measurement of at least 400 grains (Figure 3B). The order of average grain size for these samples is 5ALD<BM<CR. SEM micrographs obtained for 0ALD, 3ALD, 5ALD, 7ALD, BM, and CR at >92% relative density (Figure 4) show Al_2O_3 inclusions (dark spots) in the microstructure of 3-7ALD, indicating that the solubility of Al_2O_3 in YSZ is <1.4 wt% (3ALD). The number of Al_2O_3 inclusions increased with increasing Al_2O_3 content.

3.4 | Intermediate stage densification kinetics

Young and Cutler⁴¹ were the first to determine the activation energy of sintering from CRH experiments. Expanding upon this quantitative analysis of CRH experiments, Wang and Raj^{22,23} separated the sintering rate equation into density, grain size, and temperature-dependent terms to determine the apparent activation energy (Q) from multiple CRH experiments:

$$\ln \left[T \left(\frac{dT}{dt} \right) \left(\frac{d\rho}{dt} \right) \right] = \frac{-Q}{RT} + \alpha \quad (2)$$

$$\alpha = \ln[f(\rho)] + \ln \frac{C\gamma V^{2/3}}{R} - n \ln(d) \quad (3)$$

where T is absolute temperature, dT/dt the rate of heating, ρ the relative density, R the gas constant, $f(\rho)$ a function of relative density, γ the surface energy, n the grain size power law (3 for lattice diffusion, and 4 for grain-boundary diffusion), d the grain size, V the molar volume, and C a constant. Using CRH experiments at various heating rates, Q can be determined from the slope of an Arrhenius plot of $\ln[T(d\rho/dT)(dT/dt)]$ vs $1/T$ at fixed relative densities (Equation 2). The analysis requires that grain size remain

nearly constant over the course of the experiment so that $d\rho/dT$ is approximately independent of grain size. For the systems of interest, grain size remained approximately constant until the relative density reached ~80% (Figure 3A), so Q was determined for densities <80%. The hindrance of the initial stage of sintering, which we attribute to the completeness of the ALD films deposited with 5 or more ALD cycles in this study, complicated the determination of Q during the initial stage of densification. Therefore, the relative density range chosen for the activation energy analysis was 60%-80%, which comprises the intermediate stage of densification and yielded small standard errors in the determination of the average Q . The resulting Arrhenius plots are shown in Figure S3, where each line indicates a least-squares fit to the Arrhenius expression (Equation 2) at a fixed relative density over the four heating rates considered. For each sample, the slope of this fit was evaluated at 20 relative densities ranging from 60% to 80% relative density. The slopes were then averaged over this density range to obtain a Q for each sample type (Figure 5). Q for 0ALD was found to be 665 ± 48 kJ/mol, compared with 580 and 615 ± 80 kJ/mol determined by Song et al⁴² and Wang and Raj,²³ respectively. Adding Al_2O_3 decreased the intermediate stage of densification temperatures and lowered Q until it reached a minimum value of 414 ± 74 kJ/mol for 5ALD. The addition of Al_2O_3 beyond 2.2 wt% (5ALD) increased the peak densification rate and Q .

A thin, conformal Al_2O_3 film was initially deposited at the surface of each YSZ particle using Particle ALD, thus ensuring a homogeneous distribution of Al_2O_3 throughout the green body. Conventionally, large Al_2O_3 particles ($\geq 0.1 \mu\text{m}$) are mechanically mixed with YSZ,^{10-12,18,24,43} inevitably resulting in a heterogeneous distribution of Al_2O_3 throughout the green body. To compare with the ALD-coated samples, we mechanically mixed Al_2O_3 nanopowder (13 nm) with YSZ powder to maximize the dispersion of Al_2O_3 in the green body using a conventional incorporation approach (BM). The intermediate stage densification kinetics for 5ALD and BM were found to be nearly identical, suggesting that the increased dispersion of Al_2O_3 in the green

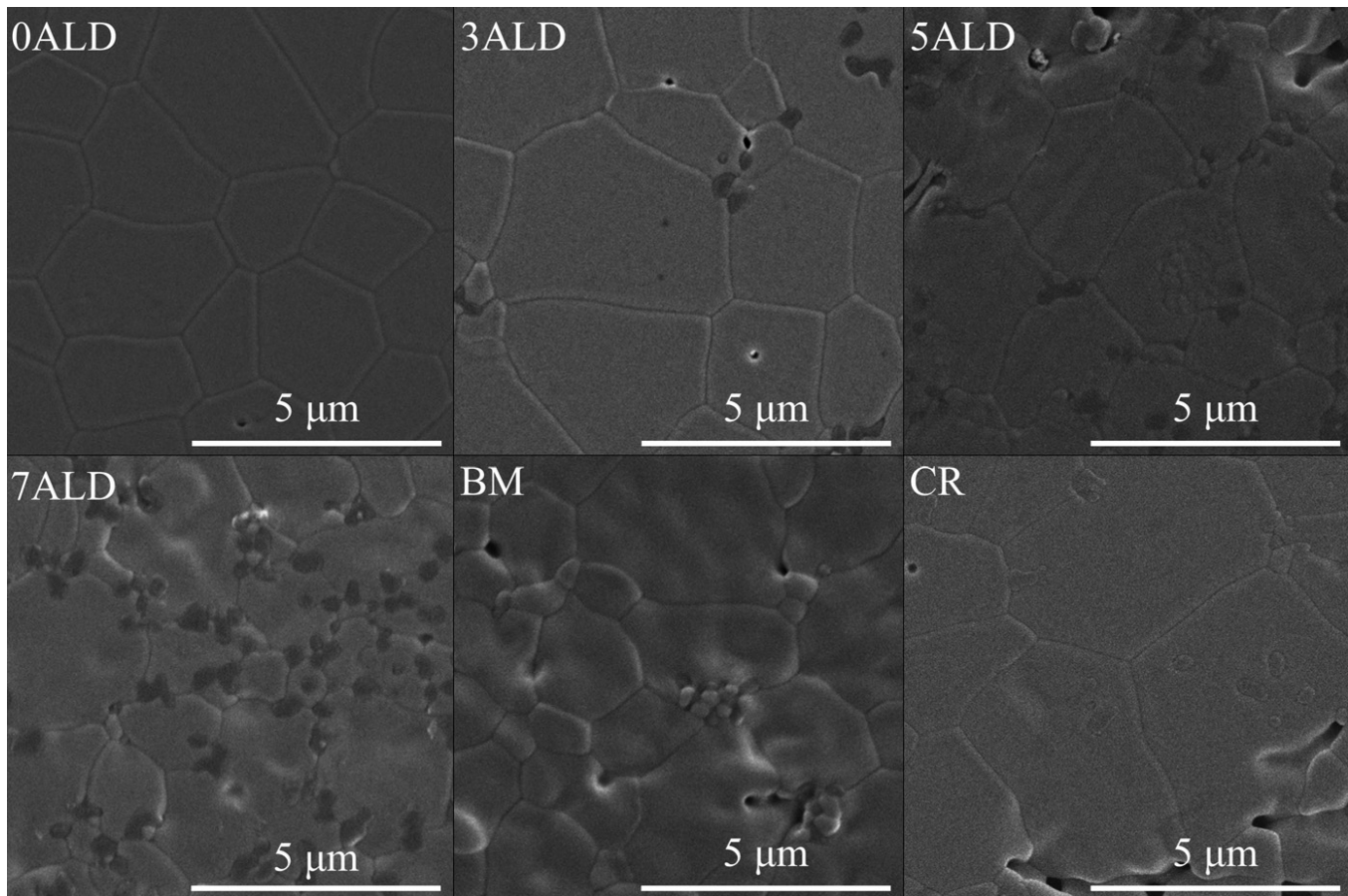


FIGURE 4 SEM images of 0ALD, 3ALD, 5ALD, 7ALD, BM, and CR for samples sintered at 1450°C for 2 hours and thermally etched at 1400°C for 30 minutes

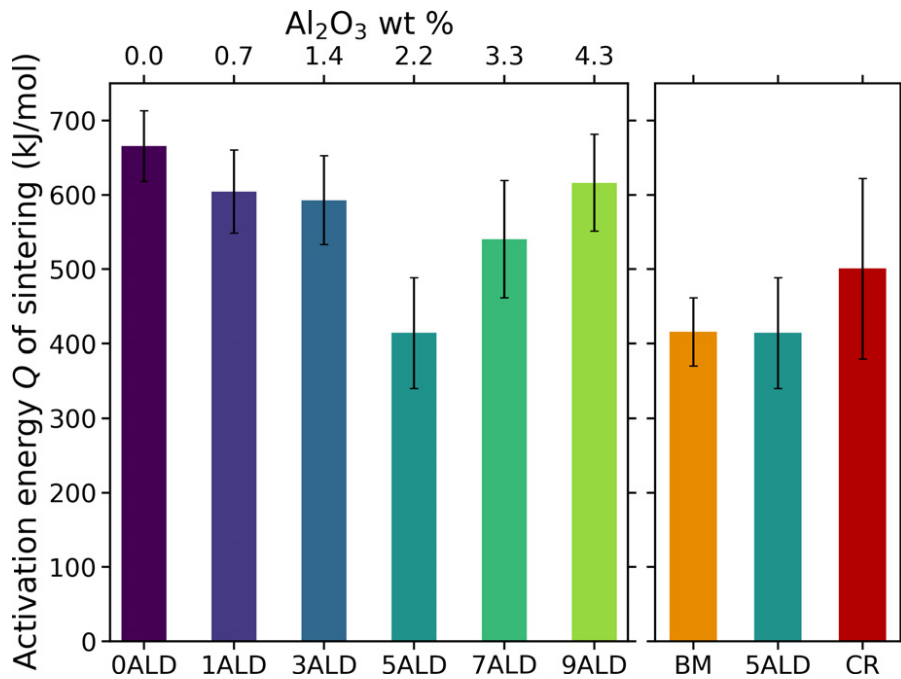


FIGURE 5 Apparent activation energy Q of each sample type resulting from the Arrhenius analysis depicted in Figure S3 [Color figure can be viewed at wileyonlinelibrary.com]

body of samples composed of ALD-coated particles does not enhance the kinetics of this process compared with the conventional incorporation of Al_2O_3 nanopowder by ball

milling. From this, we conclude that the mobility of Al^{3+} cations must be sufficiently high to overcome greater diffusion lengths from localized regions with high Al^{3+}

concentrations to regions with low Al^{3+} concentrations that results from mechanical mixing and thus the diffusion of Al^{3+} cations is not the controlling mechanism for densification during the intermediate densification stage. By comparing intermediate stage densification kinetics for YSZ with Al_2O_3 added as an amorphous film (5ALD) or a crystalline film (CR), the effect of film structure on densification was assessed. We observed no significant difference in Q for 5ALD and CR (Figure 5), so film crystallinity does not significantly impact the diffusion of Zr^{4+} cations during the intermediate stage of densification.

3.5 | Mechanisms of densification

Compared with the pure YSZ sample, the addition of 2.2 wt% Al_2O_3 decreased Q by ~40% (Figure 5). The increased diffusion kinetics caused by the addition of Al_2O_3 can be attributed to the enhancement of either volume diffusion (VD) or grain-boundary diffusion (GBD). It is well established that the densification of pure YSZ occurs by GBD and the addition of a small quantity (~0.25 wt%) of Al_2O_3 activates VD^{14,15} because the dissolution of aliovalent Al^{3+} cations into the YSZ lattice decreases the $\text{Zr}^{4+}\text{-O}^{2-}$ bond strength.¹⁹ However, the reported values for Al_2O_3 solubility in the ZrO_2 or YSZ lattice vary from <0.3 to 1 wt% Al_2O_3 ,^{9,16–18} considerably less than the 2.2 wt% Al_2O_3 where the most significant rate enhancement was observed.

The minimization of Q for the case of 2.2 wt% Al_2O_3 addition, which far exceeds the solubility limit, indicates that Al_2O_3 enhances YSZ densification beyond an activation of VD. Song et al⁴² stated that Al^{3+} cation segregation will “soften” grain boundaries and enhance grain-boundary diffusivity and mobility. Matsui et al⁴⁴ quantified grain boundary segregation in Y-TZP (3 mol% Y_2O_3 -doped ZrO_2) and found the average Al_2O_3 concentration to be ~1.5 wt% over a width of ~6 nm at the grain-boundary interface. Using this information, we estimated the amount of Al_2O_3 required to saturate the grain boundaries and grain interior. Assuming a 14-sided tetrakaidecahedron geometry, we used equations reported by Zhao and Harmer⁴⁵ to determine the volume fraction of grain boundaries with segregated Al_2O_3 ($V_{f,gb}$):

$$V_{f,gb} = \frac{(12\sqrt{3} + 6) t}{8 d} \quad (4)$$

where d is the average grain size during the intermediate stage of densification (0.176 μm), and t is the grain-boundary segregation thickness (6 nm). If the solubilities of Al_2O_3 in the grain boundary and grain interior are 1.5 and 1 wt%, respectively, the maximum dissolution of Al_2O_3 into the YSZ lattice and grain boundaries would only be ~1.1 wt%. Therefore, Al^{3+} cation segregation at the grain boundaries alone likely does not explain the benefits of

adding >1.1 wt% Al_2O_3 and certainly does not account for the enhanced densification kinetics above 2 wt% Al_2O_3 as shown in this work.

Similar to the results of this study, Suárez and Sakka¹⁵ found that the addition of 0.65–2.16 wt% Al_2O_3 to YSZ caused a reduction in Q relative to pure YSZ during the initial stage of densification. They attributed the enhancement in sintering rate to a mechanism shift from GBD for pure YSZ to VD for Al_2O_3 -doped YSZ. At 2.16 wt% Al_2O_3 addition, Al_2O_3 does not completely dissolve into the YSZ lattice to enable VD, however, it was reasoned that the dominant mechanism remains VD for a limited amount of Al_2O_3 addition beyond the solubility limit. Simply attributing the decrease in Q to the mechanistic shift from GBD to VD conflicts with the results of the present study. For 3ALD (1.4 wt% Al_2O_3), sufficient Al_2O_3 is present to diffuse into the lattice and segregate at the grain boundaries to promote densification by enabling VD, but Q for 3ALD is only ~11% lower than 0ALD (no Al_2O_3 addition). However, further addition of Al_2O_3 to 2.2 wt% (5ALD), caused Q to decrease by ~40% relative to 0ALD, indicating significant enhancement of intermediate stage densification. Destabilization of the YSZ lattice by Al^{3+} cations and segregation of Al^{3+} cations to the grain boundaries at the given solubility limits do not explain the decrease in Q observed when the amount of Al_2O_3 was increased from 1.4 to 2.2 wt%, as the maximum dissolution of Al_2O_3 into the grain interior and at the grain boundary is likely reached at ≤ 1.4 wt% Al_2O_3 (ie, ≤ 3 ALD cycles). If Al_2O_3 is present in concentrations exceeding its solubility limit, Al_2O_3 will be present at the grain boundaries as an intergranular amorphous phase or around the YSZ grains as bulk Al_2O_3 . Previous work suggested that there is no intergranular amorphous phase for Y-TZP densified with Al_2O_3 ,^{44,46} so the excess Al_2O_3 is likely present as bulk Al_2O_3 which was observed in SEM micrographs for samples with Al_2O_3 content ≥ 1.4 wt% (Figure 4). Because VD is only affected by the dissolution of Al^{3+} cations into the YSZ lattice, no known mechanism exists by which bulk Al_2O_3 around the YSZ grains enhances VD. Therefore, the observed decrease in Q upon increasing the Al_2O_3 content from 1.4 to 2.2 wt% could likely only result from the enhancement of GBD caused by the presence of a small amount of Al_2O_3 in the intergranular regions between YSZ particles.

Intergranular Al_2O_3 has two opposing effects on densification. Grain-boundary pinning by Al_2O_3 inclusions decreases grain size which decreases the diffusion distances for Zr^{4+} cations travelling from grain boundaries to pores, enhancing densification.³⁹ However, Al_2O_3 inclusions can also act as a diffusion barrier for migrating Zr^{4+} cations, hindering densification.^{15,42} After sintering at 1150°C for 2 hours (59%–67% relative density), the order of grain size

is $0\text{ALD} < 3\text{ALD} \approx 5\text{ALD} \approx 7\text{ALD}$, suggesting that the dissolution of Al_2O_3 into the grain boundaries enhances grain growth at these intermediate densities. However, after sintering at 1350°C (81%–89% relative density) intergranular Al_2O_3 slows grain growth at the end of the intermediate stage and the order becomes $0\text{ALD} < 7\text{ALD} < 5\text{ALD} < 3\text{ALD}$. Samples with small amount of Al_2O_3 inclusions (3–7ALD) experience a decrease in Q as the relative density increases to 80%, whereas samples with less Al_2O_3 than the solubility limit (0ALD and 1ALD) experience an increase in Q (Figure S3). This supports that as the relative density approaches 80%, the Al_2O_3 inclusions hinder grain growth and decrease Zr^{4+} cation diffusion distances, and consequently Q , as the Al_2O_3 content is increased to 2.2 wt% (5ALD). However, at Al_2O_3 concentrations >2.2 wt%, the large number of intergranular Al_2O_3 inclusions inhibit sintering by blocking the diffusion of Zr^{4+} cations travelling along the grain boundaries. This is reflected in this work for 7ALD (3.3 wt% Al_2O_3) and 9ALD (4.3 wt% Al_2O_3) where densification was hindered in the intermediate stage. Al_2O_3 addition affects densification through multiple mechanisms, where the extent of its effect on densification is a function of the Al_2O_3 concentration. Thus, 2.2 wt% Al_2O_3 addition may optimize densification kinetics because sufficient Al_2O_3 is present to dissolve into the lattice and grain boundaries (enhancing VD and GBD) and to situate in-between YSZ grains to control grain growth without significantly blocking Zr^{4+} cation diffusion (decreasing the diffusion path length for Zr^{4+} cations).

3.6 | Ionic conductivity

Yttria-stabilized zirconia is a promising SOFC electrolyte material because of its high oxygen ion (O^{2-}) conductivity at elevated temperatures (700–850°C). However, the high sintering temperature required to adequately densify YSZ increases manufacturing costs and can lead to degradation of the anode during co-firing.¹¹ Consequently, there is considerable interest in reducing the sintering temperature of YSZ by incorporating sintering aids that do not have detrimental effects on the ionic conductivity. In order to evaluate the efficacy of materials in this study as industrially-viable SOFC electrolytes, 0ALD, 1ALD, 5ALD, and BM were sintered at a reduced temperature of 1350°C (compared with the standard, 1450°C) for 2 hours prior to triplicate ionic conductivity measurements by AC impedance spectroscopy (Figure 6; filled markers). The lowest ionic conductivity we measured at 850°C was 0.026 S/cm for pure YSZ (0ALD), while the addition of 0.7 wt% Al_2O_3 (1ALD) increased the ionic conductivity by 23% to 0.032 S/cm, the highest ionic conductivity we found for all sample types. Addition of 2.2 wt% Al_2O_3 by Particle ALD (5ALD) or mechanical mixing (BM) reduced the ionic

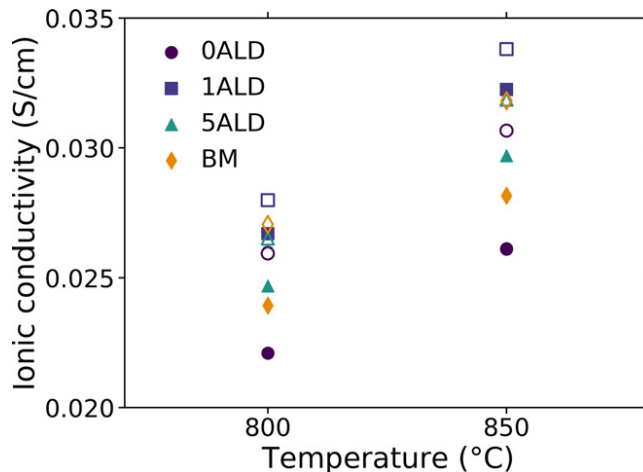


FIGURE 6 Average ionic conductivity measurements for 0ALD, 1ALD, 5ALD, and BM sintered at 1350°C for 2 hours, where closed markers (●, ■, ▲, ◆) indicate measured ionic conductivity and open markers (○, □, △, ◇) indicate adjusted conductivity. The standard error for triplicate experiments was $<3\%$ for all sample types and temperatures [Color figure can be viewed at wileyonlinelibrary.com]

conductivity compared with 1ALD, although it did improve the ionic conductivity relative to the 0ALD sample.

The addition of small quantities of Al_2O_3 to YSZ reduced the sintering temperature required to reach $>85\%$ relative density by $\sim 75^\circ\text{C}$ (Figure 2A–B). Because the sintering temperature prior to AC impedance measurements was only 1350°C , 0ALD reached a final density of only 92.6% (Table 1). During the CRH experiments (Figure 2D), the densification rate of BM was found to be hindered during the final stage of sintering. This effect is also observed for the isothermal sintering at 1350°C where BM reached a final density of only 93.8%, whereas 1ALD and 5ALD reached higher densities of 97.2% and 96.1%, respectively. Open porosity in YSZ leads to a reduction in ionic conductivity, which is reflected by 0ALD and BM exhibiting lower conductivities than 1ALD and 5ALD.

The addition of 0.7 wt% Al_2O_3 by Particle ALD (1ALD) results in the highest ionic conductivity of the samples evaluated. This is consistent with previous findings, where a maximum ionic conductivity is found at ~ 1

TABLE 1 Average final densities of samples tested for ionic conductivity (0ALD, 1ALD, 5ALD, and BM) after sintering at 1350°C for 2 hours

Sample	Relative density (% theoretical)
0ALD	92.6 ± 0.3
1ALD	97.2 ± 0.6
5ALD	96.1 ± 0.1
BM	93.8 ± 0.9

wt% Al_2O_3 .^{7,10,11} Al_2O_3 addition has two primary competing effects on the ionic conductivity of YSZ—the enhanced sinterability of Al_2O_3 -containing samples leads to higher final densities, facilitating higher conductivities, but the formation of insulating Al_2O_3 inclusions at the YSZ grain boundaries block diffusion of O^{2-} ions, decreasing the observed conductivity.⁹ At 0.7 wt% Al_2O_3 addition (1ALD), sufficient Al_2O_3 is present to enhance sinterability, which causes an increase in the final density and ionic conductivity relative to pure YSZ (0ALD). Increasing the Al_2O_3 content from 0.7 to 2.2 wt% (5ALD) does not further increase the final density but does increase the concentration of insulating Al_2O_3 inclusions present at the grain boundaries, which decreases the ionic conductivity. Therefore, 1ALD exhibits the highest ionic conductivity of the samples examined after low temperature sintering because it reaches a high final density with the least amount of Al_2O_3 addition.

To study the effect of Al_2O_3 dissolution on ionic conductivity, we adjusted the observed ionic conductivities (σ) to correct for insulating pores and Al_2O_3 addition using the equation reported by Nomura et al⁴⁷:

$$\sigma_{adj} = \frac{\sigma}{2(0.01d_{rel} - 0.5)} \quad (5)$$

where σ_{adj} is the adjusted ionic conductivity and d_{rel} is the relative density accounting for both pores and Al_2O_3 addition (Figure 6; open markers). At all concentrations evaluated, the addition of Al_2O_3 increased the adjusted ionic conductivity relative to pure YSZ, in agreement with the findings of Yu et al.¹⁰ The presence of Al_2O_3 during sintering is known to help mitigate the resistive effects of SiO_2 impurities in YSZ by scavenging to the grain boundaries.^{8,9,48} This contributes to the increase in σ_{adj} for the samples containing Al_2O_3 . Even after correcting ionic conductivity for Al_2O_3 inclusions and porosity, 1ALD (0.7 wt% Al_2O_3 addition) had the highest σ_{adj} . It has been reported that the addition of <1 wt% Al_2O_3 (1ALD) enhances YSZ grain growth through Al^{3+} cation dissolution into grain boundaries. However, at higher Al_2O_3 concentrations (5ALD and BM), undissolved Al_2O_3 pins grain boundaries, increasing the total resistive grain-boundary area in the final microstructure.^{10,12,38} This caused the observed reduction in the adjusted ionic conductivities of 5ALD and BM compared with 1ALD. Therefore, 1ALD exhibits both the highest ionic conductivity and adjusted ionic conductivity of the samples examined because enough Al_2O_3 is present to scavenge SiO_2 impurities, and enhance sinterability and grain growth without the formation of insulating Al_2O_3 inclusions. Coating YSZ powder using a single Al_2O_3 ALD cycle is a fast process that is easily scaled for large batches and does not require the use of solvents, in contrast to conventional mixing processes.²⁷ The results of this

work show that Particle ALD is a viable process for YSZ/ Al_2O_3 SOFC electrolyte material production with comparable ionic conductivity and sintering behavior to powders processed by conventional methods.

4 | CONCLUSIONS

Particle ALD was used to conformally coat YSZ powder with Al_2O_3 films of varying thicknesses, homogeneously dispersing the Al_2O_3 sintering aid throughout the green body. The sintering behavior, microstructural evolution, and ionic conductivity of materials formed from these powders were evaluated and compared with those formed from YSZ powder with Al_2O_3 added by mechanical mixing. The results of this study led to the following conclusions:

- The addition of Al_2O_3 , either by mechanical mixing or Particle ALD, resulted in a reduction in the sintering temperature required to reach a high final density by $\sim 75^\circ\text{C}$. However, the initial location, phase, and quantity of sintering aid in the green body significantly impacts sintering behavior. The presence of an Al_2O_3 film between adjacent YSZ particles impedes neck formation and hinders the onset of densification, and this effect is most pronounced for samples with the thickest Al_2O_3 films (7ALD and 9ALD). Samples with Al_2O_3 added as a crystalline film (CR) or particles (BM) experienced enhanced grain growth during the final stage of densification relative to samples with Al_2O_3 added as an amorphous film at the same concentration (5ALD). Enhanced grain growth caused pores to break away from grain boundaries during sintering which reduced the final density of BM and CR.
- A minimum apparent activation energy, Q , for the intermediate stage of densification was found for 2.2 wt% Al_2O_3 addition, and no significant difference in Q was found for equivalent amounts of Al_2O_3 addition by Particle ALD and mechanical mixing. The dissolution of Al_2O_3 into the YSZ lattice and grain boundaries has been cited as the reason for densification enhancement. However, the minimum Q was found for Al_2O_3 addition well in excess of the solubility limit of Al_2O_3 in YSZ, and it is likely that a small quantity of bulk Al_2O_3 in the microstructure also enhances intermediate stage densification kinetics by hindering grain growth through grain-boundary pinning which reduced the diffusion path length for Zr^{4+} cations.
- The highest ionic conductivity for the samples sintered at a reduced temperature of 1350°C for 2 hours was found for YSZ coated using one Al_2O_3 ALD cycle (0.7 wt% Al_2O_3), which increased the ionic conductivity by 23% relative to pure YSZ. Conductivity is maximized

when sufficient Al_2O_3 is present to achieve a high final density while limited amounts of bulk Al_2O_3 are present in the final microstructure to impede ionic diffusion. YSZ powder with Al_2O_3 addition by Particle ALD led to an enhancement in ionic conductivity relative to YSZ powder mechanically mixed with crystalline Al_2O_3 , which can be attributed to the higher final relative density associated with the deposition of amorphous Al_2O_3 .

ACKNOWLEDGMENTS

The authors are grateful for the support of the National Science Foundation [GOALI #1563537]. We also thank Fredrick Luiszer (University of Colorado Boulder) for performing ICP analysis, EAG Laboratories for performing HRTEM and TEM EDS and Tomoko Borsa and Melanie Hopek (University of Colorado Boulder) for SEM support.

CONFLICT OF INTEREST

A.W. Weimer has a significant financial interest in ALD NanoSolutions, Inc.

ORCID

Rebecca J. O'Toole  <http://orcid.org/0000-0001-8785-206X>

Sandrine Ricote  <http://orcid.org/0000-0001-7565-0284>

Alan W. Weimer  <http://orcid.org/0000-0002-2471-349X>

REFERENCES

- Singhal SC. Advances in solid oxide fuel cell technology. *Solid State Ionics*. 2000;135(1):305–13.
- Stetter JR, Penrose WR, Yao S. Sensors, chemical sensors, electrochemical sensors, and ECS. *J Electrochem Soc*. 2003;150(2):S11–6.
- Ebbesen SD, Mogensen M. Electrolysis of carbon dioxide in solid oxide electrolysis cells. *J Power Sources*. 2009;193(1):349–58.
- Tao Y, Ebbesen SD, Mogensen MB. Degradation of solid oxide cells during co-electrolysis of steam and carbon dioxide at high current densities. *J Power Sources*. 2016;328:452–62.
- Hui S, Roller J, Yick S, Zhang X, Decès-Petit C, Xie Y, et al. A brief review of the ionic conductivity enhancement for selected oxide electrolytes. *J Power Sources*. 2007;172(2):493–502.
- Dong Y, Qi L, Li J, Chen IW. A computational study of yttria-stabilized zirconia: II. Cation diffusion. *Acta Mater*. 2017;126:438–50.
- Mori M, Yoshikawa M, Itoh H, Abe T. Effect of alumina on sintering behavior and electrical conductivity of high-purity yttria-stabilized zirconia. *J Am Ceram Soc*. 1994;77(8):2217–9.
- Lee JH, Mori T, Li JG, Ikegami T, Komatsu M, Haneda H. Improvement of grain-boundary conductivity of 8 mol % yttria-stabilized zirconia by precursor scavenging of siliceous phase. *J Electrochem Soc*. 2000;147(7):2822–9.
- Feighery AJ, Irvine JTS. Effect of alumina additions upon electrical properties of 8 mol.% yttria-stabilised zirconia. *Solid State Ionics*. 1999;121(1):209–16.
- Yu F, Xiao J, Lei L, Cai W, Zhang Y, Liu J, et al. Effects of doping alumina on the electrical and sintering performances of yttrium-stabilized-zirconia. *Solid State Ionics*. 2016;289:28–34.
- Lei L, Bai Y, Liu J. Ni-based anode-supported Al_2O_3 -doped- Y_2O_3 -stabilized ZrO_2 thin electrolyte solid oxide fuel cells with Y_2O_3 -stabilized ZrO_2 buffer layer. *J Power Sources*. 2014;248:1312–9.
- Tekeli S, Kayış A, Gürü M. Microstructural, mechanical and electrical properties of alumina-doped cubic zirconia (c- ZrO_2). *J Solid State Electrochem*. 2008;12(7):791–7.
- Choi SR, Bansal NP. Mechanical behavior of zirconia/alumina composites. *Ceram Int*. 2005;31(1):39–46.
- Matsui K, Tanaka K, Enomoto N, Hojo J. Sintering kinetics at constant rates of heating: effect of alumina on the initial sintering stage of yttria-stabilized cubic zirconia powder. *J Ceram Soc Jpn*. 2006;114(1333):763–8.
- Suárez G, Sakka Y. Effect of alumina addition on initial sintering of cubic ZrO_2 (8YSZ). *Ceram Int*. 2010;36(3):879–85.
- Stough MA, Hellmann JR. Solid solubility and precipitation in a single-crystal alumina-zirconia system. *J Am Ceram Soc*. 2002;85(12):2895–902.
- Levin EM, McMurdie F. Al_2O_3 - ZrO_2 . In: Ondik H, McMurdie H, editors. *Phase diagrams for zirconium and zirconia systems*. American Ceramic Society, 1998. p. 63.
- Tekeli S, Erdogan M, Aktas B. Influence of α - Al_2O_3 addition on sintering and grain growth behaviour of 8 mol% Y_2O_3 -stabilised cubic zirconia (c- ZrO_2). *Ceram Int*. 2004;30(8):2203–9.
- Boniecki M, Natanzon Y, Łodziana Z. Effect of cation doping on lattice and grain boundary diffusion in superplastic yttria-stabilized tetragonal zirconia. *J Eur Ceram Soc*. 2010;30(3):657–68.
- German R. *Liquid phase sintering*. New York, NY: Springer Science + Business; 1985.
- Matsui K, Yamakawa T, Uehara M, Enomoto N, Hojo J. Mechanism of alumina-enhanced sintering of fine zirconia powder: influence of alumina concentration on the initial stage sintering. *J Am Ceram Soc*. 2008;91(6):1888–97.
- Wang J, Raj R. Estimate of the activation energies for boundary diffusion from rate-controlled sintering of pure alumina, and alumina doped with zirconia or titania. *J Am Ceram Soc*. 1990;73(5):1172–5.
- Wang J, Raj R. Activation energy for the sintering of two-phase alumina/zirconia ceramics. *J Am Ceram Soc*. 1991;74(8):1959–63.
- Tekeli S, Demir U. Colloidal processing, sintering and static grain growth behaviour of alumina-doped cubic zirconia. *Ceram Int*. 2005;31(7):973–80.
- Hodgson SNB, Cawley J, Clubley M. The role of Al_2O_3 impurities on the microstructure and properties of Y-TZP. *J Mater Process Technol*. 1999;92:85–90.
- Matsui K, Yamakawa T, Uehara M, Enomoto N, Hojo J. Sintering mechanism of fine zirconia powders with alumina added by powder mixing and chemical processes. *J Mater Sci*. 2008;43(8):2745–53.
- King DM, Liang X, Weimer AW. Functionalization of fine particles using atomic and molecular layer deposition. *Powder Technol*. 2012;221:13–25.
- George SM. Atomic layer deposition: an overview. *Chem Rev*. 2010;110(1):111–31.

29. O'Neill BJ, Jackson DHK, Lee J, Canlas C, Stair PC, Marshall CL, et al. Catalyst design with atomic layer deposition. *ACS Catal.* 2015;5(3):1804–25.
30. Meng X, Yang X-Q, Sun X. Emerging applications of atomic layer deposition for lithium-ion battery studies. *Adv Mater.* 2012;24(27):3589–615.
31. King DM, Spencer JA, Liang X, Hakim LF, Weimer AW. Atomic layer deposition on particles using a fluidized bed reactor with in situ mass spectrometry. *Surf Coat Technol.* 2007;201(22):9163–71.
32. Puurunen RL. Surface chemistry of atomic layer deposition: a case study for the trimethylaluminum/water process. *J Appl Phys.* 2005;97(12):121301.
33. Liang X, Li N-H, Weimer AW. Template-directed synthesis of porous alumina particles with precise wall thickness control via atomic layer deposition. *Microporous Mesoporous Mater.* 2012;149(1):106–10.
34. Maca K, Pouchly V, Boccaccini AR. Sintering densification curve – a practical approach for its construction from dilatometric shrinkage data. *Sci Sinter.* 2008;40(2):117–22.
35. Mendelson ML. Average grain size in polycrystalline ceramics. *J Am Ceram Soc.* 1969;52(8):443–6.
36. Wank JR, George SM, Weimer AW. Coating fine nickel particles with Al₂O₃ utilizing an atomic layer deposition-fluidized bed reactor (ALD–FBR). *J Am Ceram Soc.* 2004;87(4):762–5.
37. Liang X, Zhan G-D, King DM, McCormick JA, Zhang J, George SM, et al. Alumina atomic layer deposition nanocoatings on primary diamond particles using a fluidized bed reactor. *Diamond Relat Mater.* 2008;17(2):185–9.
38. Guo X, Yuan R. Roles of alumina in zirconia-based solid electrolyte. *J Mater Sci.* 1995;30(4):923–31.
39. Rahaman MN. *Sintering of ceramics*. Boca Raton, FL: CRC Press, 2007; p. 110.
40. Matsubara H. Computer simulation studies on sintering and grain growth. *J Ceram Soc Jpn.* 2005;113(1316):263–8.
41. Young WS, Cutler IB. Initial sintering with constant rates of heating. *J Am Ceram Soc.* 1970;53(12):659–63.
42. Song X, Lu J, Zhang T, Ma J. Two-stage master sintering curve approach to sintering kinetics of undoped and Al₂O₃-doped 8 mol% yttria-stabilized cubic zirconia. *J Am Ceram Soc.* 2011;94(4):1053–9.
43. Suzuki TS, Sakka Y, Morita K, Hiraga K. Enhanced superplasticity in a alumina-containing zirconia prepared by colloidal processing. *Scripta Mater.* 2000;43(8):705–10.
44. Matsui K, Ohmichi N, Ohgai M, Yoshida H, Ikuhara Y. Effect of alumina-doping on grain boundary segregation-induced phase transformation in yttria-stabilized tetragonal zirconia polycrystal. *J Mater Res.* 2006;21(9):2278–89.
45. Zhao J, Harmer MP. Effect of pore distribution on microstructure development: I, matrix pores. *J Am Ceram Soc.* 1988;71(2):113–20.
46. Matsui K, Horikoshi H, Ohmichi N, Ohgai M, Yoshida H, Ikuhara Y. Cubic-formation and grain-growth mechanisms in tetragonal zirconia polycrystal. *J Am Ceram Soc.* 2003;86(8):1401–8.
47. Nomura K, Takeuchi T, Kamo S-I, Kageyama H, Miyazaki Y. Proton conduction in doped LaScO₃ perovskites. *Solid State Ionics.* 2004;175(1):553–5.
48. Butler EP, Drennan J. Microstructural analysis of sintered high-conductivity zirconia with Al₂O₃ additions. *J Am Ceram Soc.* 1982;65(10):474–8.

SUPPORTING INFORMATION

Additional supporting information may be found online in the Supporting Information section at the end of the article.

How to cite this article: O'Toole RJ, Bartel CJ, Kudas MU, et al. Particle atomic layer deposition of alumina for sintering yttria-stabilized cubic zirconia. *J Am Ceram Soc.* 2019;102:2283–2293. <https://doi.org/10.1111/jace.16091>